Top-down measurements of contact resistivity.

Bart van Pelt

April 1, 2022

Contents

1 Scratchpad

LaTeXstuff to test goes here. Also serves as usage examples.

Sheet resistance $R_{\square}$ in text.

AlOx Al_2O_3 in text.

This is my goal: some custom TODO block, with some following text for testing Lets test it: TODO: achieve goal.

2 Introduction

In the previous part of this thesis, the contact resistivity of Al-doped zinc-oxide on doped silicon was investigated, while omitting details on the performed measurements. In this part of this thesis, the devised measurement setup and method will be described in full detail. The method provides an alternative to typical contact resistivity measurements, in which several processing steps are needed to create accurately shaped contacts on the samples of interest. These methods include the Cox and Strack (C&S) and Transmission Line Method (TLM) methods, which will be explained later. Not only are these steps time-consuming and complicated to perform, they pose limitations on the types of samples that can be used. Furthermore, thermal and chemical processing steps could alter the electrical properties of the contact of interest, and there is no guarantee that the tested contacts accurately resemble the contact as it would behave in a practical device. At the start of this project a simple measurement method was suggested, coat a sample with a thin film of silver, drive a current between the top and bottom of this sample and measure the resulting potential difference. Multiplying the obtained resistance by the area of the sample should then give the specific resistance of the sample. While this suggested pin-to-plate measurement is very easy to perform, not needing any patterning and etching steps as required by C&S and TLM, it quickly became clear that the method was so unreliable that useful data could not be obtained. As the C&S and TLM methods provide some significant challenges, the choice was made to look deeper into the pin-to-plate method, and see if it can be improved on enough to be useful. This work presents a solution to this problem, in which custom printed circuit boards are used to control the current flow in the samples. With this controlled current flow

The method devised here is able to characterize samples without the need of these patterning steps, requiring only a metallization step to ensure good contacts between the probes and the sample.

3 Background

3.1 Contact resistivity

In solar cells, contact resistance can be an important loss mechanism, limiting cell efficiency. As a result, it is an important parameter to minimize. While the total contact resistance can be defined as $R_c = \frac{V}{I}$, with V and I being the voltage along the contact and the total current respectively, this changes with contact area. A more useful quantity is the contact resistivity, also known as specific contact resistance, which is area independent. This ρ_c is defined not using the total current, but the current density J:

$$\rho_c = \left.\frac{\partial V}{\partial J}\right|_{V=0}. \tag{1}$$

While from a theoretical point of view this description of contacts in terms of $J(V)$ sounds perfectly reasonable, its usage can be challenging in practice. To understand the problem, consider preparing a sample of area A and assuming that the current is uniformly distributed along the contact. The definition then easily translates to $\rho_c = \frac{V}{I}A$, where the total current I and induced voltage V can be measured. In reality, the current distribution into a contact can be localized near the edge of the contact, an effect called current crowding[3]. The current density decays exponentially with characteristic length $L_t = \sqrt{\frac{\rho_c}{R_\square}}$, called the transfer length, here $R_\square$ is the sheet resistance of the wafer. This phenomenon is illustrated in Figure 1.

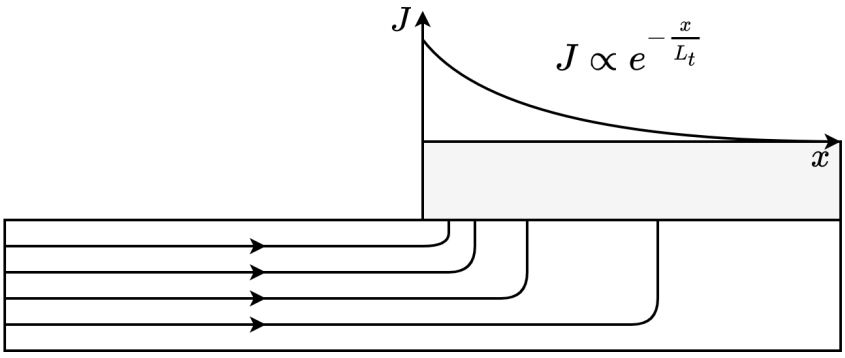

Figure 1: Illustration of current crowding along the edge of a contact. The current density J decays exponentially with distance from the contact edge. Shown are a wafer and a contact, current flows into the wafer from the left and into the contact, as indicated by the arrows.

This effect will be explained in more detail in Chapter 4, but first, let's think about its experimental implications. If the transfer length is much larger than the contacts, then the current will effectively be equally distributed. Sadly, for the samples used in this work, the transfer length was often found to be smaller than the contact dimensions. In such cases measuring V and J is not trivial, as they can vary greatly within the contact. In contrast to these locally defined V and J, it is typically only the total current, I, and *some* induced voltage, V_M, that can be measured experimentally. This is the main challenge of contact resistivity measurements: reliably distilling local $J(V)$ behaviour from global $I(V_M)$ measurements. In the next sections some typical solutions to this challenge will be discussed. Sadly, most of these methods involve patterning and etching, which, as discussed, can be difficult for ZnO:Al. TODO: does the next part fit here? Within the context of this project, symmetric lifetime samples were often made, consisting of a substrate with ZnO:Al deposited on both sides. These are further processed by thermal annealing after optional deposition of an Al_2O_3 capping layer. As this capped etching step is one of the focuses of this work, it is desirable to not change this process too much for contact resistivity samples. This is the main motivation for this part of this thesis, to figure out a way to quantify the contact resistivity of Si-ZnO:Al contacts using the available lifetime samples, without needing to drastically alter them.

3.2 Typical measurement methods

3.2.1 Cox and Strack

In the Cox and Strack (C&S) method[4] samples are made that feature circular contacts of varying size on one side of the sample, while the other side has a full backplane contact, as illustrated in Figure 2.

The resistance between the backplane and the circular contacts is then measured for the different circular contacts. The main assumption here is that the total resistance can be described as a sum of three resistances: contact resistance R_c, spreading resistance R_s, and some fixed residual resistance R_0. Cox and Strack originally modeled these terms as

$$R_T \approx \underbrace{\frac{\rho_W}{\pi d} \arctan\left(\frac{4t}{d}\right)}_{R_s} + \underbrace{\frac{\rho_c}{\frac{1}{4}\pi d^2}}_{R_c} + R_0, \tag{2}$$

where d is the diameter of the contact, ρ_W is the wafer resistivity, ρ_c the contact resistivity and t is the thickness of the wafer [2]. While more accurate

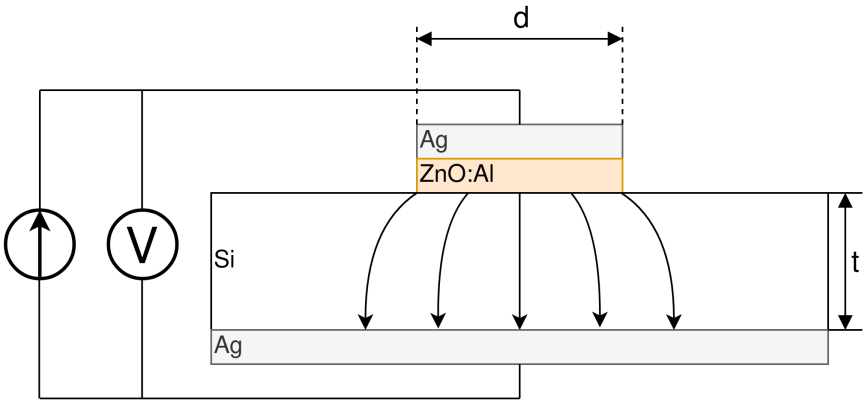

Figure 2: Illustration of a Cox and Strack measurement setup, the ZnO:Al and covering Ag layers are circularly shaped with diameter d, the Si and bottom Ag layers are much larger than the circular contact. t indicates the thickness of the Si layer. In practice, a single sample would be covered by multiple dots of varying diameter. The spreading resistance in the silicon scales differently with d than the contact resistance does, so that it can be fit out with sufficient data points.

models for the resistance terms have been found [5, 1], this form is sufficient for explaining the method. Since the contact and spreading resistances depend differently on the contact radius, the contact resistivity can be determined by varying d and fitting to the model. The practical implications of this method are that samples have to be precisely made, the circular contacts are typically tens of micrometers in radius. To make structures like this one would need to remove part of the contacting layer, for the delicate ZnO:Al films considered in this work this is known to be difficult. Not only are these extra processing steps difficult to perform, they are incompatible with typical solar cell processes, so the question remains whether the fabricated samples accurately resemble the films in solar cell processes.

3.2.2 Transmission line method

The transmission line method (TLM) somewhat resembles the C&S method in the sense that multiple sample geometries are used to fit out the contact resistivity. In TLM, the chosen geometry is typically linear, with rectangular contacts spaced at different distances, as illustrated in Figure 3.

In this setup the total resistance consists of twice the contact resistance R_c and the resistance of the Si wafer R_w. The wafer resistance can be

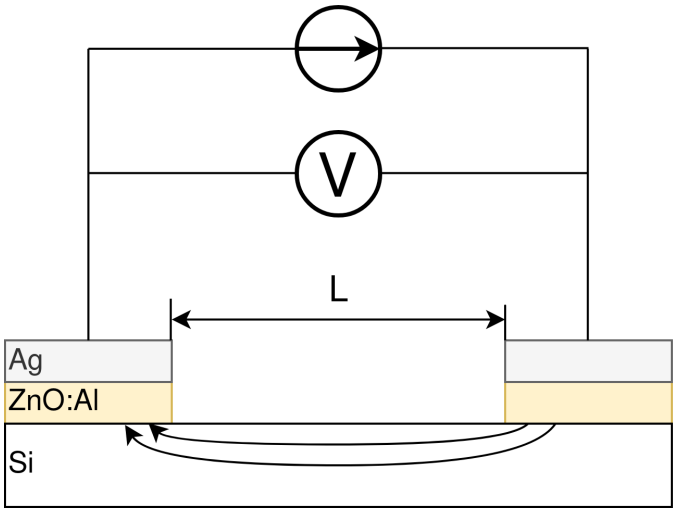

Figure 3: Side view illustration of a TLM measurement setup, on a rectangular sample of width W (not shown) several rectangular contacts are made, two shown here. The distance L between the contacts is varied. Note that the current is not uniformly distributed over the contact, but is localized within a transfer length L_t.

expressed as

$$R_w = \frac{LR_\square}{W}, \tag{3}$$

in which W is the width of the sample and $R_\square$ is the sheet resistance of the wafer.

Within the contact, the currents are localized to within a spreading length $L_t = \sqrt{\frac{\rho_c}{R_\square}}$ of the contact edge, this so-called current crowding effect will be discussed in more detail in the theory chapter of this thesis. This current crowding implies that the contact has an effective area of WL_t. Now take for the contact resistance $R_c = \frac{\rho_c}{WL_t} = \frac{R_\square L_t}{W}$, where the definition of spreading length was used to obtain the second expression. Now the total resistance can be expressed as

$$R_T = 2\underbrace{\frac{R_\square L_t}{W}}_{R_c} + \underbrace{\frac{LR_\square}{W}}_{R_w} = \frac{R_\square}{W}(2L_t + L). \tag{4}$$

Here, the horizontal and vertical intercepts signify twice the transfer length and twice the contact resistance respectively, as shown in Figure 4.

After finding the intercepts, the specific contact resistivity can be found as $\rho_c = R_c L_t W$.

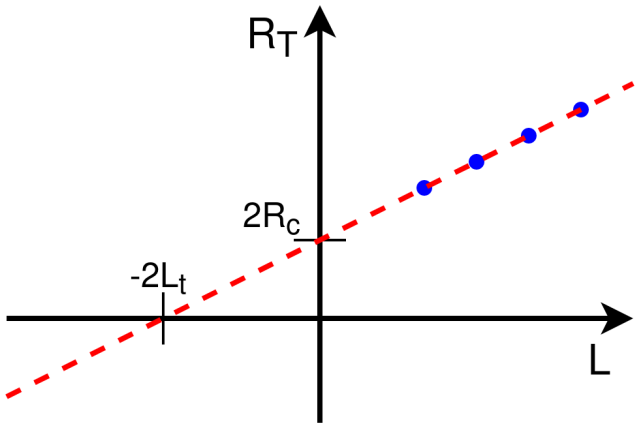

Figure 4: Example of a TLM analysis, the red fit line intercepts the horizontal axis at $-2L_t$ and the vertical axis at $2R_c$.

The drawbacks of this method are similar to those of the C&S method, patterning and etching steps are required, making TLM not only difficult, but also possibly undermining the validity of the obtained results. Again, the ZnO:Al film should be partially removed in a controlled way, something that proves challenging with typical etchants. A difference with the C&S method is that TLM samples imply symmetric measurements of a contact, in Ohmic contacts this is not an issue, but since in TLM the contacts are always in an antiseries configuration, this can make non-Ohmic contacts difficult to characterize.

3.2.3 Cross bridge Kelvin resistor

While the previously described methods rely on being able to fit out the contact resistivity from some set of measurements, the cross bridge Kelvin resistor (CBKR) method takes a different approach. In essence the method is a top-down four-terminal measurement, a current is driven from the top to the bottom of a sample using two terminals, while two other terminals are used to measure the resulting voltage.

These electrodes are formed as two L-shapes, one on either side of the sample, with the "legs" opposed to each other. One set of opposed legs is used to drive the current, while the other opposed set is used to measure the voltage. With this approach parasitic resistances are easily ignored, as the voltage measuring wires carry no current.

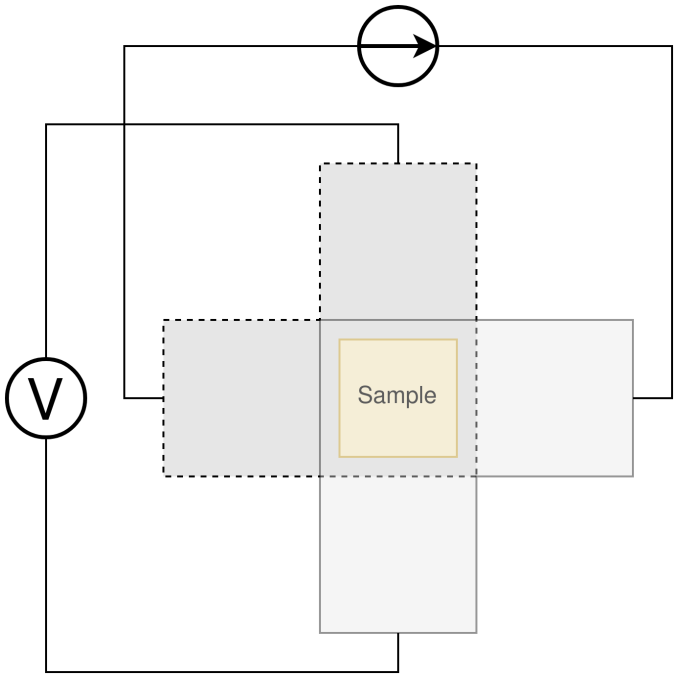

Figure 5: Illustration of a CBKR setup, shown are two L-shaped electrodes with a sample located in between. The electrodes are not in direct contact with each other. A current is driven from one of the legs of an L, through the sample, through the opposing leg of the other L. Meanwhile the resulting voltage is measured along the remaining legs. Also shown is a misalignment between the edges of the sample and the edges of the electrodes, this should ideally be small.

Measure the total resistance of the sample, and multiply this by its area to get the *measured* specific resistance,

$$\rho_M \equiv \frac{V_{\text{meas}}}{I_{\text{src}}} A, \tag{5}$$

ideally this should equal the specific resistance, ρ_c, of the sample, but this relies on some assumptions that will be checked next.

One of there assumptions is that the current is evenly distributed over the sample, or equivalently, that the contacting electrodes form isopotentials. When measuring samples with low specific resistivities this might not hold, currents can be localized near the edge of the sample, and the measured voltage might not accurately represent the average voltage across the sample. Additionally, misaligned contacts can result in currents "wrapping around" the sample, this can result in an overestimation of the average voltage over the sample.

This effect was modeled by Schreyer and Saraswat, defining the measured contact resistivity ρ_M as the product of measured resistance and sample area, and the transfer length L_t as $\sqrt{\frac{\rho_c}{R_\square}}$, their main result can be expressed as,

$$\frac{\rho_M}{\rho_c} = 1 + \underbrace{\frac{4}{3}\frac{\delta^2}{W_x W_y}\frac{A}{L_t^2}\left[1 + \frac{\delta}{2(W_x - \delta)}\right]}_{C_g}, \tag{6}$$

in which δ is the sample misalignment, and W_x and W_y are the thicknesses of the legs of the electrodes. Here the second term is referred to as the geometric correction factor, or C_g. Ideally C_g is small, so that $\rho_M \approx \rho_c$, this can be realized by using small samples, small misalignments, and highly conductive electrodes. Luckily C_g can easily be estimated. Taking $\rho_c \approx 10\text{m}\Omega\text{cm}^2$ as a lower bound, and suppose using pieces of household aluminium foil for contacts ($R_\square \approx 3\text{m}\Omega_\square$, measured with a four-point probe), this gives a worst case (i.e. shortest) transfer length of around 2 cm. For easy measurements, the needed samples should not be much smaller than a squared cm, otherwise they will be difficult to cleave and handle with tweezers. By cutting carefully, electrodes can be made with an estimated misalignment of around one mm. Substitution yields a C_g on the order of magnitude of a few thousandth's, indicating that geometric effects will not be significant in this setup.

In contrast to TLM and the C&S method, no patterning and etching steps are required by the CBKR method, making it a viable option for ZnO:Al samples. Still, there are some practical drawbacks to this method regarding the fabrication of test structures. In practice it can be difficult to cleave

samples to specified dimensions, so that electrodes need to be custom made for each sample piece to reduce misalignment. Additionally, making sure that there are no shorts between the flimsy pieces of aluminium foil can be challenging. Experience shows that strategically placed pieces of insulating tape can help, but in the end eyebrows will probably be raised when reading "we sandwiched the sample between some household foil and duct tape, and it just appeared to work" in the methods section of any report.

3.2.4 Pin to plate

The challenges of measuring contact resistivities of ZnO:Al films were known at the start of this project, previous experience showed that reliable patterning and etching of this material is difficult, making TLM and the C&S method impractical. The approach that had been used to far was to clamp samples between a copper plate and some of the probe pins of the already available four point probe setup, as illustrated in Figure 6. One of the probe pins would be used to drive a current to the plate, while another pin would be used to measure the voltage across the sample. The copper plate would serve as both a current driving electrode and a reference voltage since, due to its high conductivity, the electric fields within the plate can be assumed to be negligible.

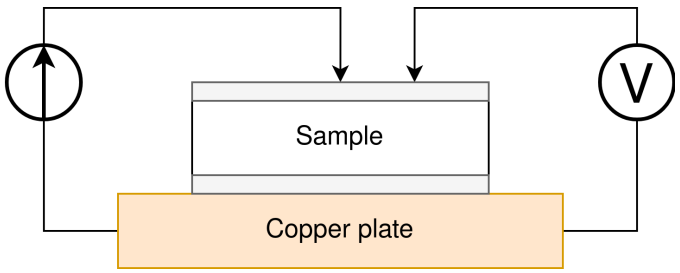

Figure 6: Illustration of a pin to plate measurement, featuring a copper base plate on which a silver coated sample is located. A current is driven between a pin and the base plate, while the voltage between another pin and the base plate is measured.

In essence this method is quite similar to the CBKR method, where a current is driven through the sample, *the* resulting voltage is measured, and the resulting resistance is multiplied by sample area to get the specific resistivity. While in the CBKR method the average voltage along the sample is measured (neglecting geometric resistance), in the pin to plate method the relation between measured voltage and average voltage is not so clear. Due to the contacting geometry, the voltage in the top contact is highly nonuniform,

so that the measured voltage can differ by orders of magnitude on a single sample, depending on where this voltage is measured.

It quickly became clear that this method provided neither reliable nor valid results, since measurements on exactly the same sample could yield values that vary by orders of magnitude. Nonetheless, the extreme ease of measurement compared to the previously discussed measurement methods made it a good candidate for further investigation. If the poorly chosen probing geometry is the cause of the problematic voltage nonuniformities, then maybe a different choice of probing geometry could solve this problem.

Addressing these challenges in the pin to plate method is the goal of the rest of this thesis. The first step is to better understand the nature of current (or equivalently, voltage, by Ohm's law) inhomogeneities, this will be the goal of Chapter 4.

4 Theory

4.1 Transfer length effects

So far, all the top-down measurement methods had to mitigate one phenomenon, transfer length effects. Consider ideal conductors used as contacts, as these form regions of equal electric potential, the potential difference between top and bottom of the sample will be equal everywhere. The driven current density will be uniform, found simply by: $J = \frac{\Delta V}{\rho_s}$. In this idealized case, contact resistivities would be trivial to measure, but in reality the driven current distributions and potential differences can be significantly inhomogeneous, as illustrated in Figure 7. To quantify these effects, the interaction between electrodes and sample was modeled, as illustrated in Figure 8.

4.1.1 Governing equations

In this model an arbitrary slab of sample and electrodes is considered, oriented along the x-y plane, with the z-direction defining the top and bottom of the setup. The electrodes are considered to be very thin, and relatively conductive, so that the voltage within each electrode are independent of z. Within these electrodes, the current density is determined by Ohm's law, so that

$$\vec{J}_{top} = -\sigma \nabla_{(x,y)} V_{top}(x,y), \tag{7}$$

and

$$\vec{J}_{bottom} = -\sigma \nabla_{(x,y)} V_{bottom}(x,y), \tag{8}$$

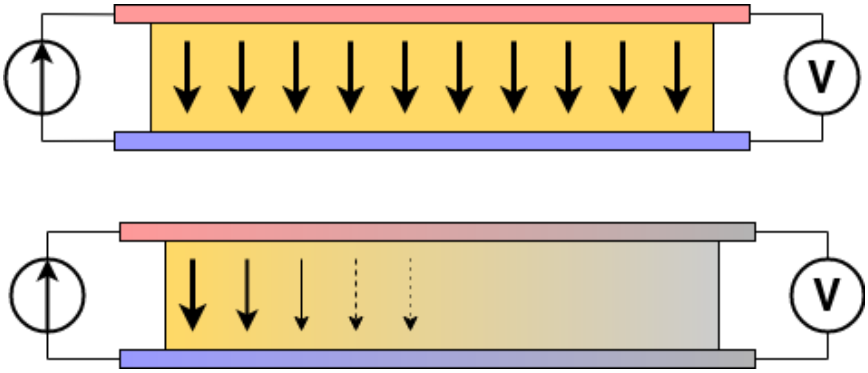

Figure 7: A comparison between contacting with ideally conducting electrodes (top) and electrodes with significant resistivity (bottom). Positive and negative voltages are shown as shades of red and blue in the electrodes, while the current density through the sample is depicted using arrows and shades of yellow. In the ideal case the contact voltages and current densities are uniform, while in the non-ideal case the current distribution is localized near the current injection point of the contacting electrodes.

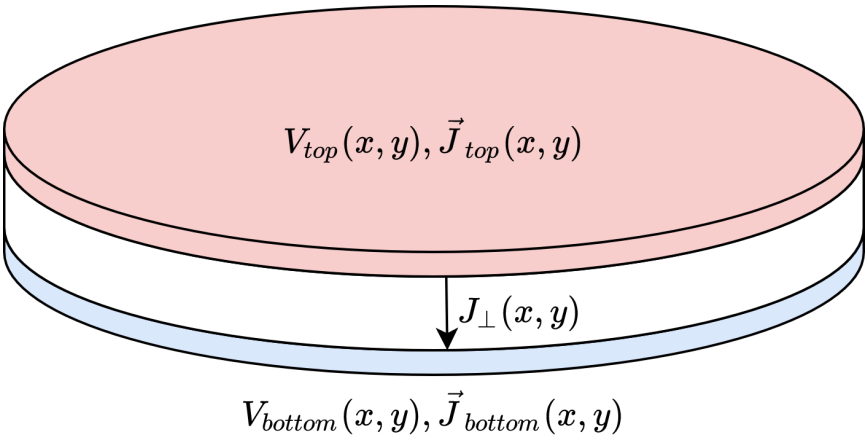

Figure 8: A model of a sample with two contacting electrodes. In the electrodes the current density is determined from the electrodes' conductivity and the electric fields. The current density through the sample can be determined from the stack resistivity ρ and the local potential difference between the top and bottom electrode.

in which σ is the conductivity of the electrode material. The current density through the sample is given by

$$J_\perp = \frac{V_{top} - V_{bottom}}{\rho}, \tag{9}$$

for some specific sample resistance ρ. Consider charge conservation in some arbitrary region Ω in the top electrode, which can be expressed as a sum of currents flowing into the region from other parts of the electrodes, and a current flowing into the sample:

$$0 = \int_\Omega \vec{J} \cdot \mathrm{d}\vec{A} = \int_\Omega J_\perp \mathrm{d}A + \oint_{\partial\Omega} \vec{J}_{top} \cdot \hat{n} h \mathrm{d}s, \tag{10}$$

where h is the thickness of the electrode. Substitution of the current densities followed by application of the divergence theorem yields

$$0 = \int_\Omega \frac{1}{\rho}(V_{top} - V_{bottom})\mathrm{d}A - \int_\Omega \sigma h \nabla^2_{(x,y)} V_{top} \mathrm{d}A, \tag{11}$$

and similarly for the bottom equation, except the sign of the $J_\perp$ contribution is switched

$$0 = \int_\Omega \frac{1}{\rho}(V_{top} - V_{bottom})\mathrm{d}A + \int_\Omega \sigma h \nabla^2_{(x,y)} V_{bottom} \mathrm{d}A. \tag{12}$$

Adding the two together, and letting $\phi \equiv V_{top} - V_{bottom}$, one gets

$$0 = \int_\Omega -\sigma h \nabla^2_{(x,y)} \phi + \frac{\phi}{\rho} \mathrm{d}A \tag{13}$$

As the choice of Ω was arbitrary, the integrand must vanish almost everywhere, so that

$$\nabla^2 \phi = \frac{R_{sq}}{\rho} \phi. \tag{14}$$

No PDE is complete without appropriate boundary conditions, in this work Neumann boundary conditions are considered, as these describe four-point probing setups the best. A current distribution is driven along some part of the domain boundary, and some resulting potential difference is measured. In dimensionless form, the equation can be written as

$$\tilde{\nabla}^2 \phi = \left(\frac{L}{L_t}\right)^2 \phi \equiv k^2 \phi, \tag{15}$$

where L is the characteristic dimension of the sample, and $L_t \equiv \sqrt{\frac{\rho}{R_{sq}}}$ is the so called transfer length, and the dimensionless Laplacian is given by $\tilde{\nabla}^2 = \frac{1}{L^2}\nabla^2$. In following sections the tilde on the Laplacian will be omitted, so that the dimensionless form of the PDE is given by

$$\nabla^2\phi = k^2\phi, \qquad \Omega \tag{16}$$

$$\nabla\phi \cdot \hat{n} = f \qquad \partial\Omega. \tag{17}$$

4.1.2 Uniqueness of solutions

To show that solutions are unique, consider two solutions, ϕ_1 and ϕ_2 and let $\hat{\phi} \equiv \phi_1 - \phi_2$, the goal will be to show that the PDE and boundary conditions force ϕ to vanish. Linearity shows that $\hat{\phi}$ must obey

$$\nabla^2\hat{\phi} = k^2\hat{\phi}, \quad \Omega \tag{18}$$

$$\nabla\hat{\phi} \cdot \hat{n} = 0 \quad \partial\Omega. \tag{19}$$

Now consider the following integral,

$$\int_\Omega \nabla \cdot (\hat{\phi}\nabla\hat{\phi})\mathrm{d}x = \oint_{\partial\Omega} \hat{\phi}\nabla\hat{\phi} \cdot \mathrm{d}\vec{A} \overset{\text{B.C.}}{=} 0, \tag{20}$$

apply the chain rule

$$0 = \int_\Omega \nabla \cdot (\hat{\phi}\nabla\hat{\phi})\mathrm{d}x = \int_\Omega \hat{\phi}\nabla^2\hat{\phi} + \nabla\hat{\phi} \cdot \nabla\hat{\phi}\mathrm{d}x, \tag{21}$$

and apply the PDE to clear the $\nabla^2\hat{\phi}$ term,

$$0 = \int_\Omega k^2\hat{\phi}^2 + \left|\nabla\hat{\phi}\right|^2 \mathrm{d}x. \tag{22}$$

With the inner product

$$\langle\phi, \psi\rangle = \int_\Omega k\phi\psi + \nabla\phi \cdot \nabla\psi\mathrm{d}x, \tag{23}$$

the result can be recognized as $0 = \langle\hat{\phi}, \hat{\phi}\rangle \Rightarrow \hat{\phi} = 0$, which proves that the solutions of the PDE are indeed unique.

4.1.3 Influence of transfer length

Now, let's solve these equations for a few geometries. The first is the simplest realizable geometry, take a sample, and contact it with pins at its center to drive the currents, while measuring a potential drop somewhere else along the sample. While in practice a rectangular sample is often used, the problem is reduced to a circular domain in order to more easily look into the spreading effects. The unit disk is chosen as a solution domain without the origin, at which the current is driven, by symmetry, this allows us to look at solutions of the form $\phi(r)$ As all currents are contained in the sample, the current density must vanish at the boundary, so that $\phi'(1) = 0$. In experimental conditions the total supplied current, I, is known. In this model however the average potential drop, $\bar{\phi}$, is specified, so that

$$\bar{\phi} = \frac{\int_\Omega \phi \mathrm{d}A}{\int_\Omega \mathrm{d}A} = \frac{2\pi}{\pi 1^2} \int_0^1 r\phi(r)\mathrm{d}r. \tag{24}$$

In the adopted cylindrical coordinates, the PDE can be expressed as

$$r^2\phi''(r) + r\phi'(r) - r^2k^2\phi(r) = 0, \tag{25}$$

which is known as the modified Bessel equation. This modified Bessel function has solutions:

$$\phi(r) = AI_0(kr) + BK_0(kr), \tag{26}$$

in which A and B are integration constants and I_0 and K_0 are modified Bessel functions of the first and second kind. By applying the boundary and integral conditions the integration constants can be found, these steps are omitted here, as it is mostly textbook linear algebra. In a simpler 1D system, the PDE reduces to $\phi'' = k^2\phi$, which was solved with a similar boundary and integral condition. The solutions are shown in Figure 9

4.2 Idea: reduce effective sample dimensions

Suppose you were to conduct a four-point probing experiment in either geometry, in which a current is driven through the sample, and some potential difference between the top and bottom of the sample, ϕ_M, is measured. What would be a good way to perform these measurements?

To answer this question, it is useful to first estimate L_t for the samples of interest. As the current distribution is least homogeneous for small L_t, it is safest to underestimate it by using large sheet resistivities and low stack resistivities. While the stack resistivity is of course not known before

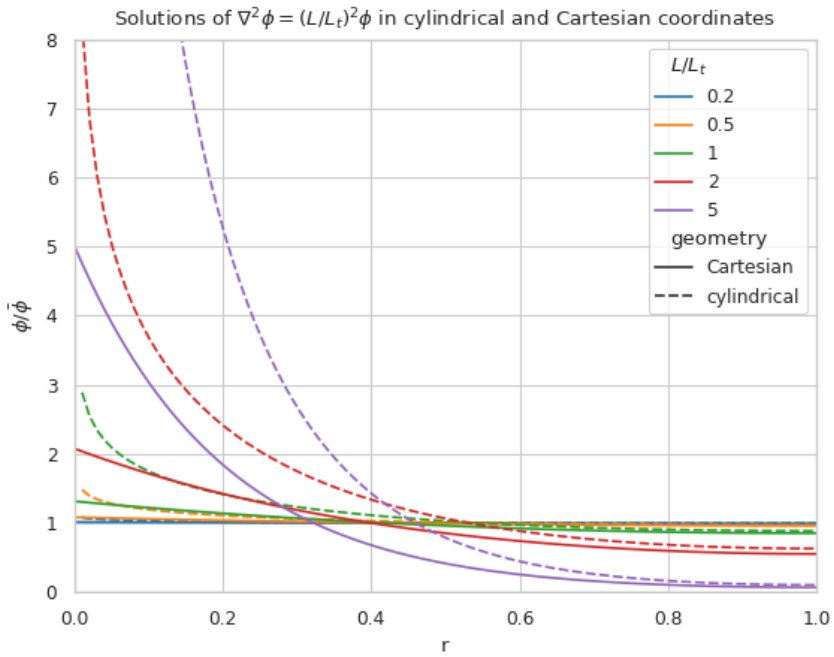

Figure 9: A comparison of solutions for ϕ on $(0, 1]$ in Cartesian and cylindrical coordinates, for varying $k \equiv \frac{L}{L_t}$. With boundary condition $\phi'(1) = 0$ and integral condition $\bar{\phi} = 1$. Note that the cylindrical solutions have much steeper gradients than the Cartesian ones, and that the homogeneity of the current distribution depends strongly on k, with large k leading to very inhomogeneous currents.

the measurements, the lowest order of magnitude of ρ was estimated at 10 mΩcm^2, while for the used AZO films, $R_{sq} \approx 100\ \Omega$ is not uncommon, in this case the transfer length is on the order of 0.1 mm.

In practice, we'd like to be able to work with samples with dimensions of at least a few mm, not just because these are easier to handle, but because these can be easily be prepared by hand-cleaving a bigger sample piece. In these cases k would be significantly larger than 1, so the majority of current will be driven only through a small part of the sample near the current drive electrode.

The goal now is to reduce k through some means, in the ideal limiting case $k = 0$, but how close is close enough? In Figure 10, the normalized value of ϕ is shown at the extremes of a sample for different k, the black horizontal line is at 99%. This shows that, in order to measure the average potential to within a percent relative error, k has to be around 0.25 or lower.

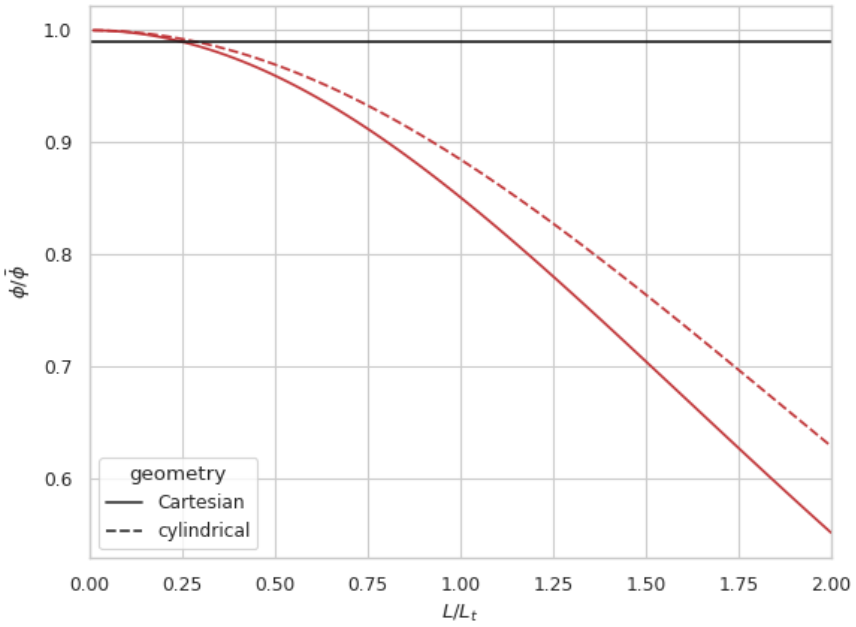

Figure 10: $\frac{\phi_M}{\bar{\phi}}$ at the edge of the sample, as function of $\frac{L}{L_t}$. For small $\frac{L}{L_t}$ the potential measured at the edge very closely resembles the average potential.

To realize this goal of decreasing $\frac{L}{L_t}$, two separate approaches are combined. The first is to increase L_t by making the contacting layers more

conductive, this is achieved by depositing 300nm of silver by e-beam evaporation. This increases L_t to approximately a few millimeters.

The second approach is to effectively reduce L by controlling the probe geometry. At first glance, L appears to be determined by the sample size, a current is driven through some point, and this current cannot flow out of the sample, represented in the boundary condition $\phi'(L) = 0$. An obvious option to reduce L could be to simply cut smaller samples, but in the millimeter range this is difficult, especially when areas need to be accurately determined. Working with tiny samples, while perfectly fine in theory, is undesired in practice, so can we decrease L in bigger samples? The answer is yes! The trick lies in the nature of the boundary condition, it is only required that $\phi'(L) = 0$, but does this imply that the sample is contained in the $0 < x < L$ range? Not neccesarily. As an example, consider the one dimensional case: $\phi''(x) = k^2\phi(x)$ on $(0, 1)$. Now instead of applying a zero flux condition at any domain edge, simply consider solutions that are symmetric around $x = \frac{1}{2}$, these can easily be constructed from the solutions, $\phi_k(x)$, shown in Figure 10, by

$$\phi_{k,\mathrm{sym}}(x) = \frac{1}{2}(\phi_k(x) + \phi_k(1 - x)). \tag{27}$$

Symmetric solutions are shown in Figure 11, it is clear that now $\phi'(\frac{1}{2}) = 0$. Notice the similarity between the solutions as shown in Figure 9 and the left half of Figure 11, they are the same! Apparently driving currents with a grid of symmetric electrodes will let us effectively change L.

5 New approach

This approach was realized using custom made printed circuit boards (PCBs), as shown in Figure 12. The PCBs feature a pad of regularly spaced copper lines, covering an area of 15 by 15 mm^2. The copper lines are alternately connected to either of the shown pins, so that they resemble interleaved combs. To perform a measurement, a sample is clamped between two such PCBs, and a current is driven between two combs on alternate sides of the sample, while the other combs are used to measure the resulting potential across the sample in a four-terminal configuration. The used copper lines were 0.6 mm wide and spaced 0.3 mm apart, with this spacing and a sample spreading length on the order of half a cm, the requirement that $\frac{L}{L_t} < 0.25$ is easily met, so that the current distribution can be considered homogeneous.

Practically, the measurements come down to the following steps:

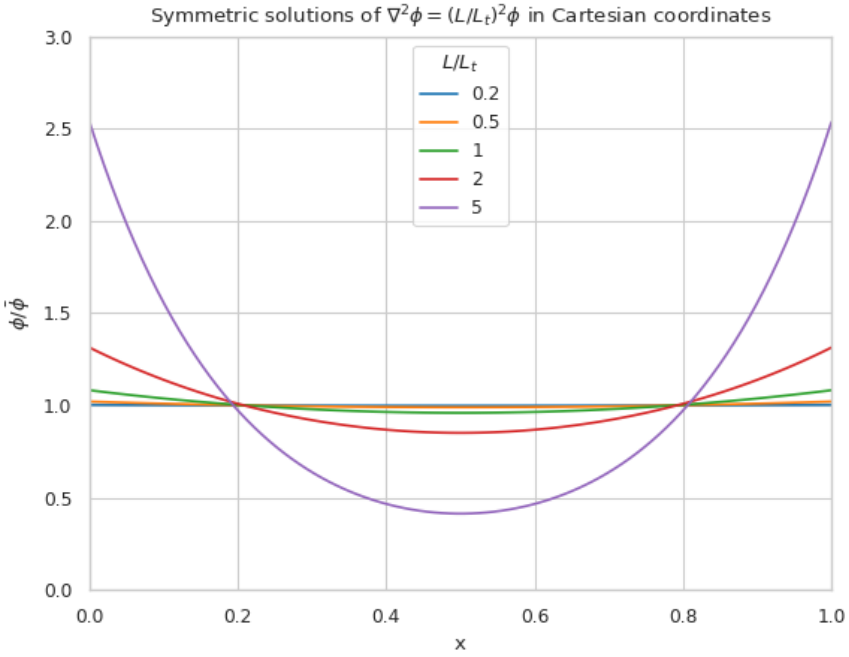

Figure 11: TODO

1. Create samples that:
    - Have a spreading length significantly larger than the distance between the fingers of the PCBs to be used. Cover with silver if neccesary.
    - Are homogeneous, this might not be the case when deposited films wrap around the samples.
    - Feature no edge deposited conductive films, it is recommended to cleave off the edges of the samples after silver deposition.
    - Have an accurately known surface area, A, in this work this was achieved with a computer vision method, which will be discussed later.
    - Fit on the 15 mm by 15 mm measurement pads of the PCBs.
2. Set up the resistance measurement system:
    - Use a sourcemeter in a four-terminal sensing configuration, in this work a Keithley 2400 was used.
    - Connect the current source terminals of the sourcemeter to "combs" on the two separate PCBs.
    - Connect the voltage measurement terminals to the remaining combs.
3. Clamp the sample between the PCBs
    - Make sure that the sample is located on the pads, and does not shift before measuring.
    - Use the alignment holes of the PCBs for consistent alignment.
    - Apply an evenly distributed pressure to the sample, this can be achieved with a glue clamp.
4. Perform a standard four-terminal resistance measurement, yielding resistance R.
5. Calculate the specific resistivity $\rho_s = R \cdot A$.

The interpretation of the measured stack resistivity depends on the used samples, as in this work symmetric samples were used, the stack resistivity must be larger than twice the interfacial resistivity of the AZO-Si interface.

In this case an upper bound on contact resistivity can be given as $\rho_c < \frac{1}{2}\rho_s$.

6 Characterization of measurement method

So far the case for PCB measurements has boiled down on purely theoretical arguments, in the following chapters the measurement method will be experimentally characterized. The characterization will focus on two desired properties of the new measurement: reliability and validity. A measurement method is reliable when it is reproducible, yielding the same results on each measurement. Reliability by itself is not enough though, simply because observations being close to each other does not imply that they are close to the *correct* value. A measurement is called valid if its results actually resemble what is **intended** to be measured. For a good measurement system these two qualities obviously go hand in hand.

While the reliability often refers to repeated measurements under the exact same conditions, this strict definition is not very useful when considering the PCB measurements, as the goal is to reliably measure the contact resistivity **without** regard to some sample handling details. For context, the initial measurement system (TODO footnote: detail pin to plate) proved quite reliable when a single sample was contacted and stayed fixed between measurements. Problems started appearing however, as soon as this sample was contacted with different pins, in slightly different locations, rotated a bit, or a different sample piece was used. The estimated contact resistivities varied unpredictably when even slight, to the user practically unnoticeable, changes were made to the setup. The goal here is not to be reliable under strict control of all influencing factors, but to be reliable in a somewhat chaotic environment, one in which the user can choose not to care about the exact shape and contacting points of their samples, and still get *reliable* results. For this reason, the term reliability is used in a looser sense in this work: a measurement is considered reliable when it yields similar (enough) results in a range of realistic usage scenarios.

More practically speaking, these "realistic usage scenarios" should at least include different contacting conditions, like where the sample is located and in which orientation, but also simply using another sample of differing dimensions. These reliability experiments were done by varying exactly the mentioned conditions and measuring if these influence the measurement, this will be discussed in more detail in following sections.

To check the validity of the measurement, a reference measurement is needed. Ideally a sample with a well known specific resistance could be used,

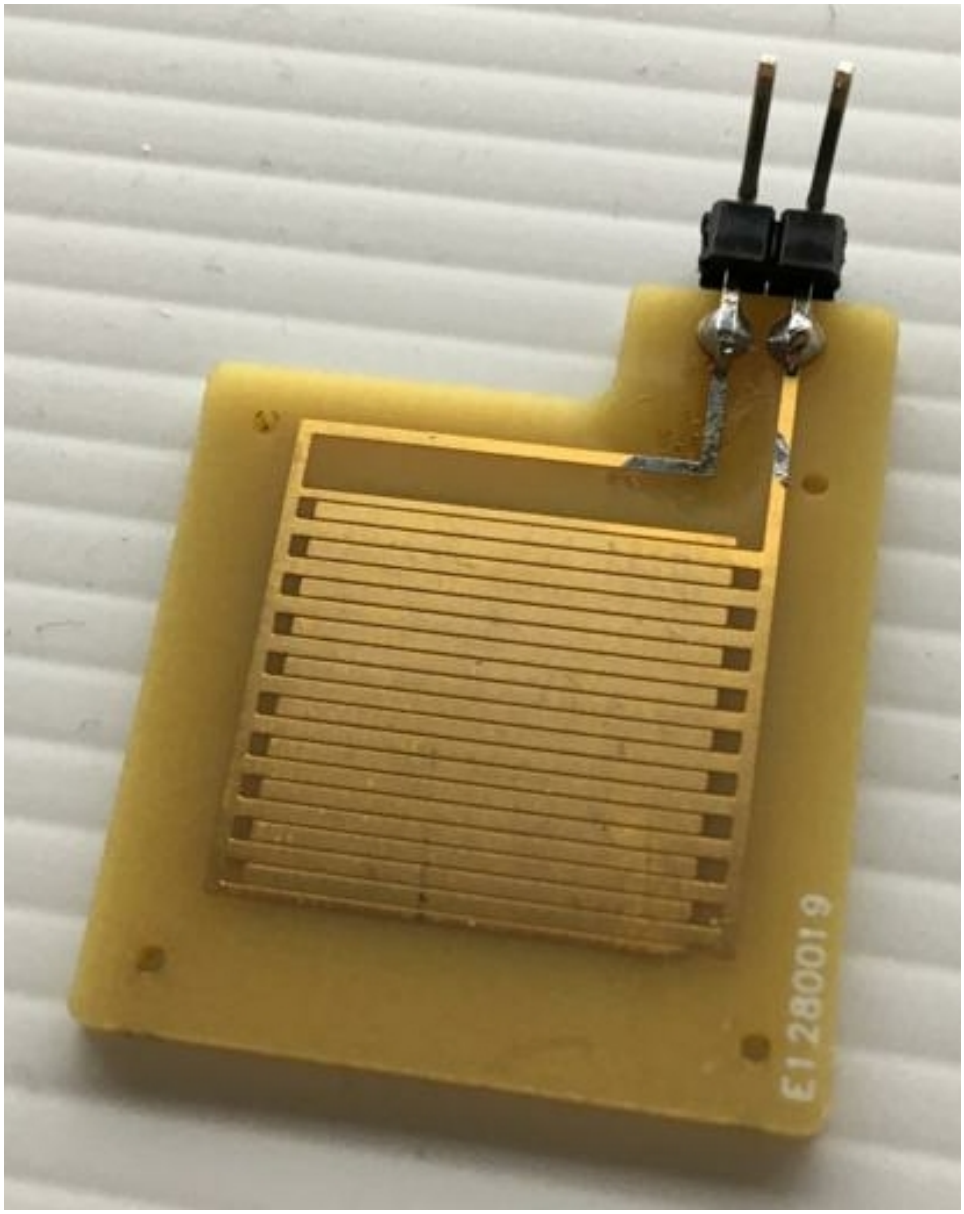

Figure 12: TODO

but these were not available. Another option is to take a sample, measure the specific resistance through some other means, and then compare the results with the new method. This concurrent validity test was chosen, in which the novel method was compared to a cross bridge kelvin resistor (CBKR). The choice for a CBKR test was made since it can handle the same type of samples that the PCBs can. The needed patterning for Cox & Strack and other methods would imply the need to make separate samples, process them differently, and just hope that they have the same specific resistance. A CBKR allows for measurements on the exact same samples as on the PCBs, without any alterations, making it fit for a direct comparison of measurement methods.

7 Results

7.1 Reliability

Ideally the PCB method should yield the same contact resistivities, regardless of

- Sample orientation,
- Sample position,
- Sample shape.

These assumptions were checked, starting with the sample orientation. Here the contact resistivity was measured for two cases, in the "long" case the long edge of the sample was aligned parallel to the fingers of the PCBs, while in the "short" case the short edge was aligned parallel to the fingers. This was done for two symmetric samples:

1. pSi substrate with r48 AZO annealed at 400C, measuring approx 4.5 mm by 6.5 mm.
2. 130 Ω n+ Si with r48 AZO annealed at 400C, measuring approx 6.5 mm by 9.0 mm.

The results are shown in Figure 13. For the pSi sample, the results are quite consistent, while for the n+ Si sample there is more spreading in the measurements. This can be explained by the pSi sample having a larger contact resistivity than the n+ Si sample, and thus a larger spreading length, this sample also happened to have smaller dimensions, so that overall the

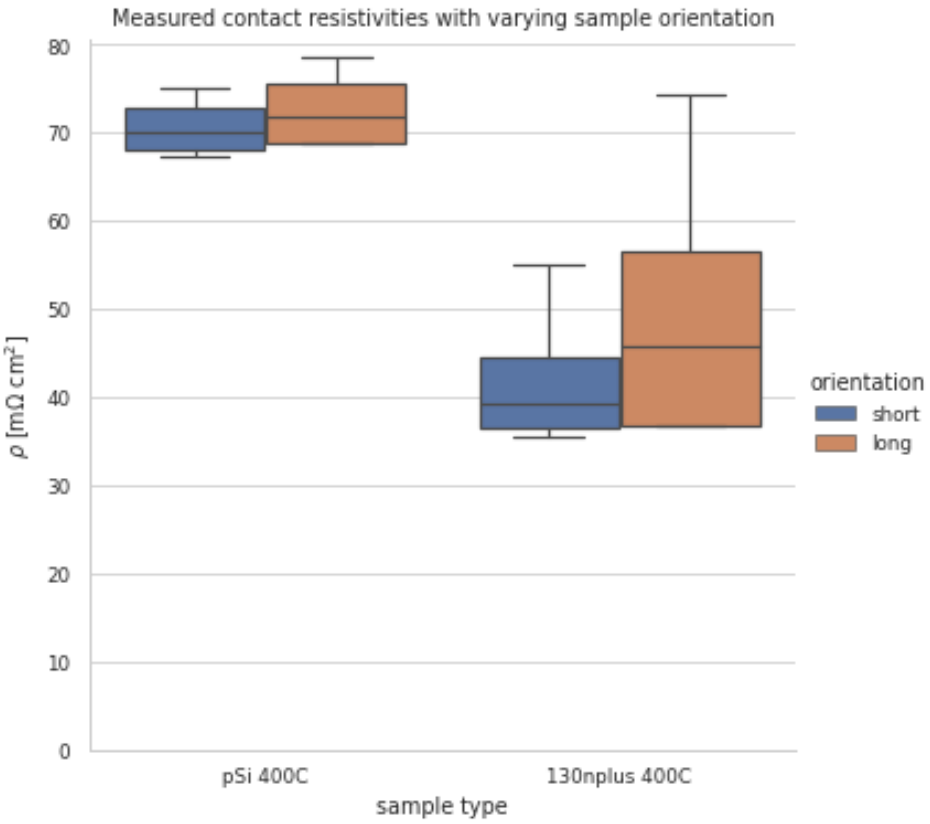

Figure 13: Measured contact resistivities with varying orientation. Two different samples were used, for which the contact resistivity was measured in different orientations. In the "short" cases, when the short side of the sample lies parallel to the PCB's fingers, the measurements are most reliable.

current distribution can be expected to be more homogeneous. Overall, the measurement seems most repeatable in the "short" configuration.

Next the location of the sample on the PCB was varied for a few samples. The samples were located at all four extreme corners of the PCB pad and at the center. Figure 14 shows the measured results for each of the tested samples, note the logarithmic vertical axis. This shows that the measurement is typically reliable on a per-sample basis. Clear are the deviations between pieces of similar samples, while these should all have the same contact resistivities, Figure 14 shows clear differences between samples which were cut out of exactly the same wafer.

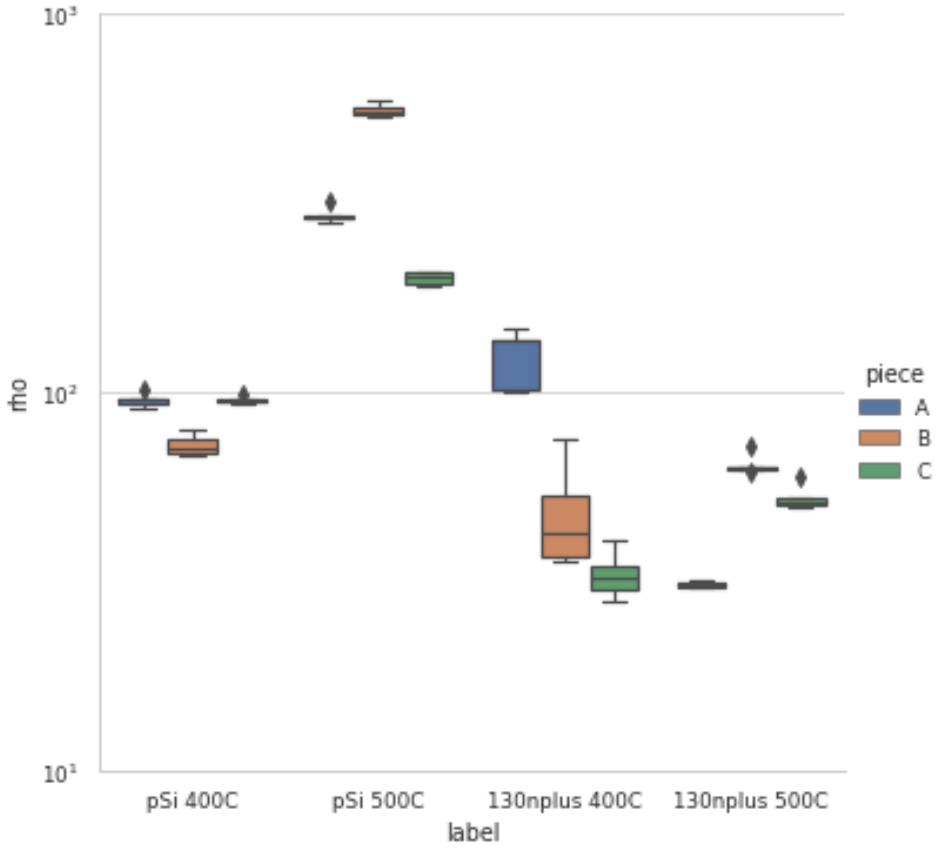

Figure 14: Measured contact resistivities of different pieces of different samples, the spread between measurements on different pieces are often larger than the spread within the pieces. This is not totally understood, but wrap-around of ALD films is expected to play a significant role.

7.2 Validity: Cross Bridge Kelvin Resistor comparison

Finally the PCB method was cross-validated with a Cross Bridge Kelvin Resistor (CBKR) setup which was carefully crafted from pieces of aluminium foil. While this alternate method is difficult and time consuming to perform, it provides a good sanity check for the PCB method. To do this, two L-shaped pieces of aluminium foil were cut, with the widths of the legs matching the dimensions of the samples. These contacting pads were made for each specific sample. Then the sample was clamped between the pieces of foil, while pieces of insulating tape ensured that no shorts could occur between the contacting pads. Two opposing "legs" were used to drive a current, while the potential difference was measured between the others, again in a four-point probe configuration. Several samples were used, for which the contact resistivity was measured multiple times with the PCB method and the CBKR method, Figure 15 shows that the results correlate strongly, here the error bars show the minimal and maximal values for each measurement.

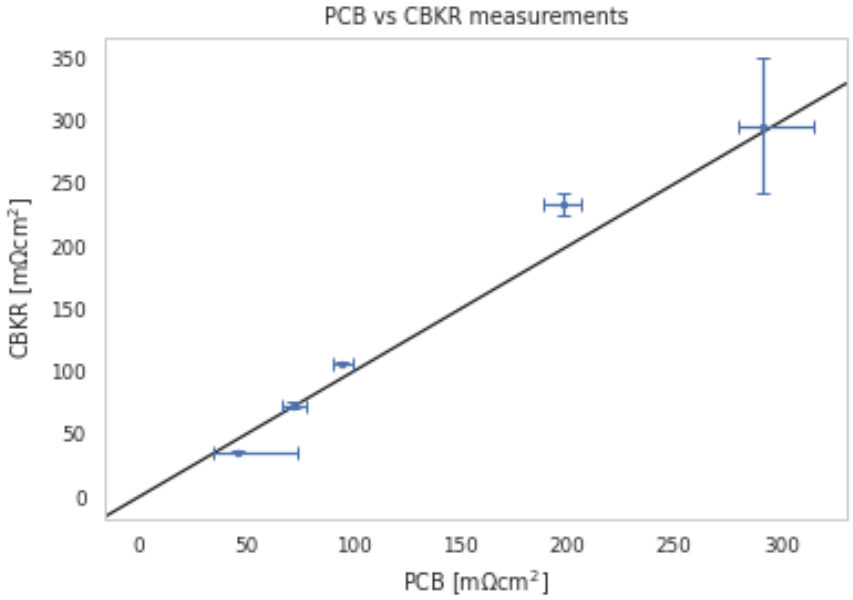

Figure 15: Comparison between PCB measurements and and CBKR measurements on a set of samples, the error bars indicate the minimum and maximum of the measured values. Ideally the measurements should match exactly, which is indicated by the black line.

8 Conclusion and outlook

A method for easy contact resistivity measurements on laterally uniform samples was developed. This was achieved by contacting samples with custom made printed circuit boards, featuring interleaved comb-like copper contacts, which are used to drive a uniform current distribution through a sample. In contrast to the Cox & Strack and transmission line methods, which involve delicate sample patterning steps, the method developed here only requires uniform conductive contacting layers. This is especially important for ZnO:Al samples, since controlled etching of these layers is known to be difficult, rendering TLM and the C&S method impractical. In essence, the new method shows similarities to the CBKR method, both methods use a four terminal approach, and both aim to eliminate inhomogeneous currents by electrode design. In contrast to the CBKR method, in which the electrode dimensions need to match the sample dimensions, the PCBs used in the new method enable a rapid reuse of the same testing structure for samples of different dimensions.

References

[1] M. Ahmad, T. Ganguli, S. Patil, S. Major, Y. G. K. Patro, and B. M. Arora. Determination of contact resistivity by a modified Cox and Strack method in case of finite metal sheet resistance. *Solid-State Electronics*, 38(8):1437–1440, Aug. 1995.

[2] R. H. Cox and H. Strack. Ohmic contacts for GaAs devices. *Solid-State Electronics*, 10(12):1213–1218, Dec. 1967.

[3] D. Schroder and D. Meier. Solar cell contact resistance—A review. *Electron Devices, IEEE Transactions on*, 31:637–647, June 1984.

[4] D. K. Schroder. *Semiconductor Material and Device Characterization*. John Wiley & Sons, Inc., Hoboken, NJ, USA, Apr. 2005.

[5] M. van Rijnbach, R. J. E. Hueting, M. Stodolny, G. Janssen, J. Melskens, and J. Schmitz. On the Accuracy of the Cox–Strack Equation and Method for Contact Resistivity Determination. *IEEE Transactions on Electron Devices*, 67(4):1757–1763, Apr. 2020.